


Ion Pairing Hot Paper

 How to cite: *Angew. Chem. Int. Ed.* **2024**, *63*, e202315381
 doi.org/10.1002/anie.202315381

Counterion Effect in Cobaltate-Catalyzed Alkene Hydrogenation

Martin Gawron, Franziska Gilch, Daniel Schmidhuber, John A. Kelly,
 Thomas M. Horsley Downie, Axel Jacobi von Wangelin, Julia Rehbein,* and Robert Wolf*

Dedicated to Professor Rhett Kempe on the occasion of his 60th birthday

Abstract: We show that counteranions exert a remarkable influence on the ability of anionic cobaltate salts to catalyze challenging alkene hydrogenations. An evaluation of the catalytic properties of [Cat][Co(η^4 -cod)₂] (Cat=K (**1**), Na (**2**), Li (**3**), (^{Dep}nacnac)Mg (**4**), and N(ⁿBu)₄ (**5**); cod=1,5-cyclooctadiene, ^{Dep}nacnac={2,6-Et₂C₆H₃NC(CH₃)₂CH}) demonstrated that the lithium salt **3** and magnesium salt **4** drastically outperform the other catalysts. Complex **4** was the most active catalyst, which readily promotes the hydrogenation of highly congested alkenes under mild conditions. A plausible catalytic mechanism is proposed based on density functional theory (DFT) investigations. Furthermore, combined molecular dynamics (MD) simulation and DFT studies were used to examine the turnover-limiting migratory insertion step. The results of these studies suggest an active co-catalytic role of the counterion in the hydrogenation reaction through the coordination to cobalt hydride intermediates.

Introduction

The hydrogenation of alkenes is among the most widely utilized reactions for the synthesis of petrochemical intermediates, fine chemicals, drugs, agrochemicals, and nutrients.^[1,2] Noble metals such as rhodium, palladium and

iridium are routinely used as catalysts owing to their high reactivity, high selectivity, mild reaction conditions, and ease of operation.^[3] However, growing environmental and economic awareness has emphasized more sustainable technologies including the use of first row transition metals due to their higher abundance in the Earth's crust.^[4] As a result, the development of effective hydrogenation protocols with Mn, Fe, Co, and Ni has gained traction over the last decade.^[5] Among them, anionic pre-catalysts, such as (ene)metalate salts (M=Fe, Co, Ni) and heteroleptic diimine cobaltates, have been shown to exhibit high catalytic activity for unbiased and bulky alkenes (Figure 1A).^[6-9] While the modular nature of such metalate pre-catalysts has enabled large variations of the ligands and metal ions, the potential of adopting counterion-sensitive mechanisms has so far not been investigated. Despite the availability of numerous anionic organometallic reagents and coordination complexes,^[10] detailed studies of counteranion effects on molecular reactivity have remained scarce and have only recently gained greater recognition.^[11,12] For example, Miller and co-workers demonstrated the cooperative effect of alkali metal cation binding in the Ir-catalyzed isomerization of allylbenzene (Figure 1B).^[13] Addition of 1–4 mol % MBAr^F₄ (M=Li, Na, K; Ar^F=3,5-bis(trifluoromethyl)phenyl) to the iridium catalyst drastically increased the rate of isomerization to β -methylstyrene with turnover frequencies ranging from 1.8 h⁻¹ (M=K) to 2000 h⁻¹ (M=Li). Kempe and co-workers observed a remarkable influence of the alkali metal cation on the manganese catalyzed imine hydrogenation (Figure 1C).^[14] Alteration of the co-catalytic alkoxide base MOⁿBu (M=K, Na, Li) accelerates the reaction following the trend: K⁺ > Na⁺ > Li⁺. An outer-sphere mechanism was proposed, in which a potassium cation actively participates in the rate-determining hydride transfer step. Similar observations have been made for Ru-catalyzed (asymmetric) Noyori-type hydrogenations.^[15]

Previous studies from our group documented a strong counterion effect in the hydrogenation of 1,5-cyclooctadiene (cod) with bis(imino)acenaphthene (BIAN) cobaltates [M-(thf)_n][(^{Dipp}BIAN)Co(η^4 -cod)] (M=Li, n=3.5; M=K, n=1) used as catalysts.^[7] Using the lithium cobaltate generated 61% cyclooctene, while the potassium analogue gave only 1%. We reasoned that such behavior could be more general and provide an additional parameter for catalyst optimization.

Herein, we report a strong counteranion effect on the catalytic hydrogenation of bulky alkenes with homoleptic

[*] M. Gawron, F. Gilch, Dr. J. A. Kelly, Dr. T. M. Horsley Downie, Prof. Dr. R. Wolf

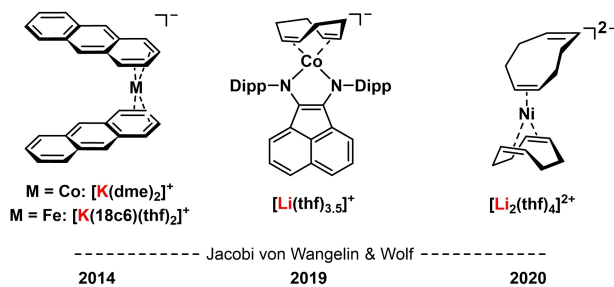
Institute of Inorganic Chemistry, University of Regensburg
 93040 Regensburg (Germany)
 E-mail: robert.wolf@ur.de

D. Schmidhuber, Prof. Dr. J. Rehbein
 Institute of Organic Chemistry, University of Regensburg
 93040 Regensburg (Germany)
 E-mail: julia.rehbein@ur.de

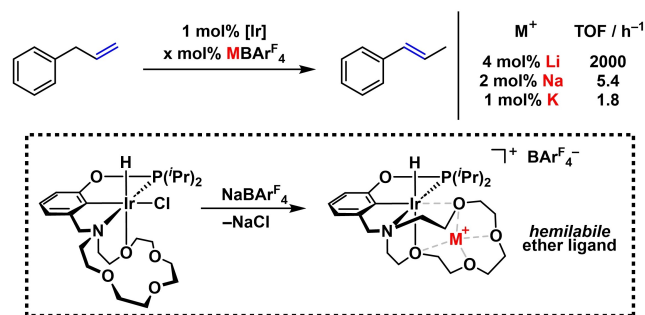
Prof. Dr. A. Jacobi von Wangelin
 Department of Chemistry, University of Hamburg
 20146 Hamburg (Germany)

© 2023 The Authors. Angewandte Chemie International Edition published by Wiley-VCH GmbH. This is an open access article under the terms of the Creative Commons Attribution Non-Commercial License, which permits use, distribution and reproduction in any medium, provided the original work is properly cited and is not used for commercial purposes.

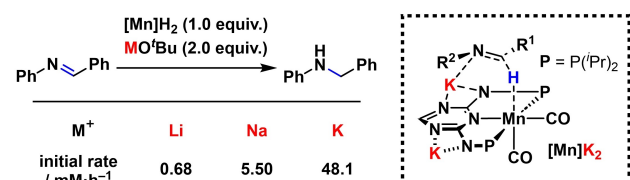
A. Anionic 3d-Transition Metal Pre-Catalysts for the Hydrogenation of Alkenes



B. Ion-Responsive Iridium Catalyzed Isomerization Reaction (Miller 2017)



C. Cation Effect in Manganese Catalyzed Imine Hydrogenation (Kempe 2019)



D. This Work: Counterion-Sensitive Cobaltate Catalyzed Alkene Hydrogenation

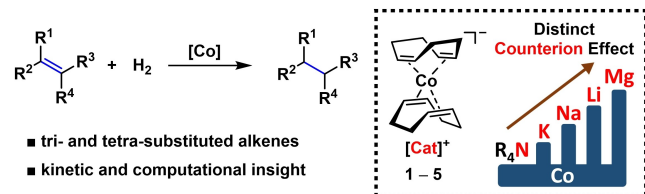


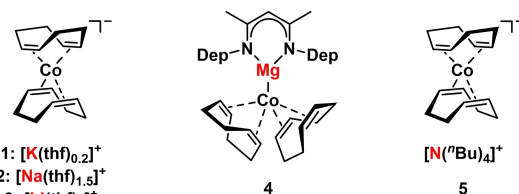
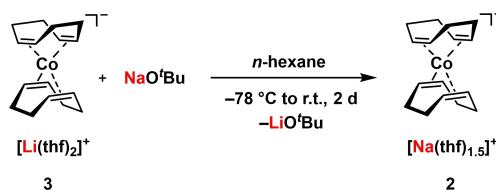
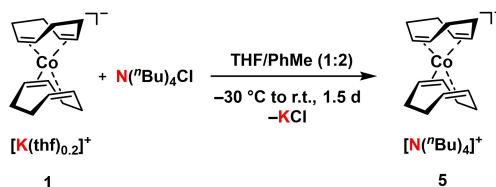
Figure 1. A: Anionic 3d-transition metalates used for alkene hydrogenation (18c6 = 18-crown-6; Dipp = 2,6-diisopropylphenyl). B: Ion-responsive iridium catalyzed isomerization reaction. C: Counterion effect in manganese catalyzed imine hydrogenation and graphical representation of the proposed rate-determining hydride transfer step. The pre-catalyst $[Mn]H_2$ carries two protons in place of the two K^+ ions in $[Mn]K_2$. D: This work: counterion-sensitive cobaltate catalyzed alkene hydrogenation.

$[Co(\eta^4-cod)_2]^-$ pre-catalysts, with the best-performing pre-catalyst bearing a magnesium counterion (Figure 1D). The topicity of the catalytic system and the reaction-time profile is investigated by H_2 uptake studies. Combined molecular dynamics (MD) and density functional theory (DFT) studies indicate an active role of the counterion in the turnover-limiting migratory insertion step *via* a $M-\mu_2-H-Co$ moiety.

Results and Discussion

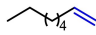
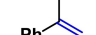
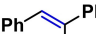
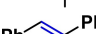

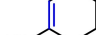
Pre-Catalyst Synthesis and Initial Evaluation of Counterion Influence

In order to systematically examine the influence of different counteranions on the catalytic potential, we synthesized a series of bis(η^4-cod)cobaltate salts $[Cat][Co(\eta^4-cod)_2]$ (Cat = $K(thf)_{0.2}$ (**1**), $Na(thf)_{1.5}$ (**2**), $Li(thf)_2$ (**3**), $(^{Dep}nacnac)Mg$ (**4**), and $N(^{t}Bu)_4$ (**5**); Scheme 1, top). While complexes **1**, **3** and **4** were readily obtained via known procedures,^[16,17] the sodium salt **2** was prepared from **3** by a cation exchange reaction with NaO^tBu in 34 % yield (Scheme 1a). Single crystal X-ray diffraction (SC-XRD) analysis on crystals grown from THF/*n*-hexane revealed the formation of a solvent-separated ion pair $[Na(thf)_6][Co(\eta^4-cod)_2]$ (Na1–Co1 8.220(7) Å; see Figure S31, SI). Substitution of the metal-based cation by reaction of **1** with equimolar $N(^{t}Bu)_4Cl$ afforded $[N(^{t}Bu)_4][Co(\eta^4-cod)_2]$ (**5**) in 28 % yield (Scheme 1b). SC-XRD analysis revealed that complex **5** shows an ion-separated structure (N1–Co1 6.207(1) Å) similar to **2** in the solid state (Figure S32, SI). A comparative study of the catalytic activities of the cobaltates **1–5** in alkene hydrogenations (2–12 bar H_2 , 30–60 °C, Table 1) revealed a clear trend of increasing activity from potassium cobaltate **1** to magnesium cobaltate **4**. 1-Octene was hydrogenated quantitatively by the Li^+ , Na^+ and $(^{Dep}nacnac)Mg^+$ salts **2–4** but to a much lower degree with the K^+ salt **1** (Table 1, entry 1). The $(^{Dep}nacnac)Mg$ cobaltate **4** gave the highest conversions in the hydrogenation of tri- and tetra-substituted alkenes

a) Preparation of **2**:b) Preparation of **5**:

Scheme 1. Top: Olefin cobaltates **1–5** tested in the hydrogenation reaction of unsaturated substrates; Dep = 2,6-diethylphenyl. Bottom: a) Preparation of $[Na(thf)_{1.5}][Co(\eta^4-cod)_2]$ (**2**); b) Preparation of $[N(^{t}Bu)_4][Co(\eta^4-cod)_2]$ (**5**).

Table 1: Hydrogenation of alkenes with olefin cobaltates 1–5.^[a]

Entry	Olefin	Yield (Conv.) [%]				
		Cat. 1	Cat. 2	Cat. 3	Cat. 4	Cat. 5
1 ^[b]		63 ^[e]	98	> 99	> 99	1 (23) ^[e]
2 ^[b]		8 (15)	76 (82)	> 99	> 99	1 (7)
3 ^[b]		1 (< 5)	5 (8)	93	> 99	0 (2)
4 ^[c]		9 (11)	20 (20)	> 99	> 99	/
5 ^[c]		4 (6)	5 (11)	72 (77)	94	/
6 ^[d]		15 (18)	2 (11)	29 (37)	81 (85)	/

[a] Standard conditions: 0.2 mmol substrate (0.4 mol/L THF). Yields and conversions were determined by quantitative GC-FID analysis vs. internal *n*-pentadecane. Conversions are given in parentheses if < 90%. [b] 3 mol% cat., 2 bar H₂, 30 °C, 3 h. [c] 5 mol% cat., 8 bar H₂, 40 °C, 22 h. [d] 5 mol% cat., 12 bar H₂, 60 °C, 22 h. [e] isomerization to internal double bonds.

(Table 1, entries 3–6), whereas the tetrabutylammonium derivative **5** showed negligible activity (Table 1, entries 1–3). To gain further insight into the reaction course, the hydrogenation of α -methylstyrene was monitored by ¹H NMR spectroscopy using [K(thf)_{0.2}][Co(η^4 -cod)₂] (**1**) and [(^Depnacnac)Mg][Co(η^4 -cod)₂] (**4**) as pre-catalysts (10 mol %, 2 bar H₂, ambient temperature, Figures S12–13, SI). These experiments confirmed that **4** is the more expedient pre-catalyst, enabling the complete hydrogenation of α -methylstyrene in < 266 min. In contrast, pre-catalyst **1** gave 24 % of cumene after 263 min. It is also important to note that well-resolved NMR spectra with sharp signals are observed until the hydrogenation reaction has ceased. This strongly indicates the absence of (paramagnetic) cobalt particles in the reaction mixtures.

Catalyst Properties of [(^Depnacnac)Mg][Co(η^4 -cod)₂] (**4**)

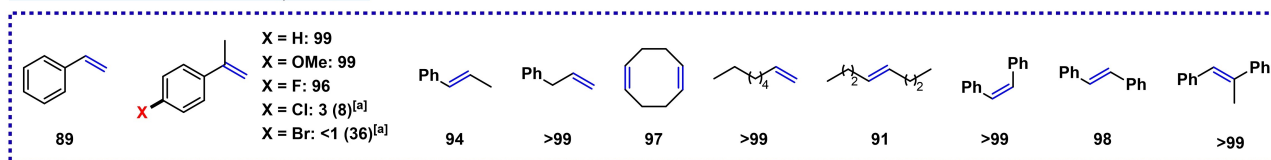
These promising findings prompted us to investigate the substrate scope for complex **4**. Following the initial screening and control experiments (see the SI), the hydrogenation of different alkenes was tested using **4**. A low catalyst loading and mild H₂ pressure (3 mol % **4**, 2 bar H₂, 30 °C, 3 h; Figure 2, Protocol A) sufficed for the hydrogenation of linear α -olefins (e.g. 1-octene, styrene) to tri-substituted olefins (e.g. trans- α -methylstilbene). In terms of functional group tolerance, α -methylstyrene substituted with 4-OMe- or 4-F groups did not impede hydrogenation, but 4-Cl and 4-Br substituents did. Using a slightly modified protocol (5 mol % **4**, 12 bar H₂, 40 °C, 22 h; Figure 2, Protocol B), more challenging tri- and tetra-substituted olefins were successfully hydrogenated. The quantitative hydrogenation of naphthalene to 1,2,3,4-tetrahydronaphthalene and the hydrogenation of the C–C σ -bond in cyclopropylbenzene

highlighted the high activity of pre-catalyst **4**. In addition, α,β -unsaturated esters underwent facile hydrogenation with high chemoselectivity for the C=C double bond showcasing an extension to functionalized alkene substrates. Finally, tetra-substituted olefins such as 2,3-dimethyl-1*H*-indene, 2-methyl-3-phenyl-1*H*-indene, 1,1,2,2-tetramethylethylene, 1-phenyl-1,2,2-trimethylethylene and even the very sterically hindered 1,1,2,2-tetraphenylethylene were hydrogenated in good to excellent yields (61–94 %).

Catalyst Topicity

Further studies focused on reaction progress analyses and kinetic poisoning experiments to distinguish between a homotopic (single molecular) vs. a heterotopic (multiple aggregated) active site.^[18] The investigations focused on complex **4**, for which the reaction progress analysis of the hydrogenation of α -methylstyrene (3 mol %, 2 bar H₂, 25 °C) showed a short induction period between 30 to 90 s (Figure 3, black curve; see the Supporting Information for further information). Initial ligand exchange with the respective alkene substrate parallel to its hydrogenation can account for the delay in reaction onset.^[19,20] This is followed by steady conversion giving > 90 % hydrogenation product after 10 min. The attempted amalgamation with excess mercury (1690 mol %, 563.3 equiv. with respect to **4**) at 0 min had only a minor effect on the reaction rate and full conversion was still reached within 20 min (Figure 3, blue curve).^[21] Use of trimethylphosphine (PMe₃, 12 mol %, 4.0 equiv. with respect to **4**) resulted in catalyst inhibition pointing to a homotopic active species (Figure 3, green curve).^[17,22] A four-fold excess of PMe₃ is necessary to occupy all the coordination sites at the Co center.^[23] Poisoning with dibenzo[*a,e*]cyclooctene (dct, 60 mol %, 20.0 equiv. with

Protocol A: 3 mol% Cat. 4, 2 bar H₂, 30 °C, 3 h



Protocol B: 5 mol% Cat. 4, 12 bar H₂, 40 °C, 22 h

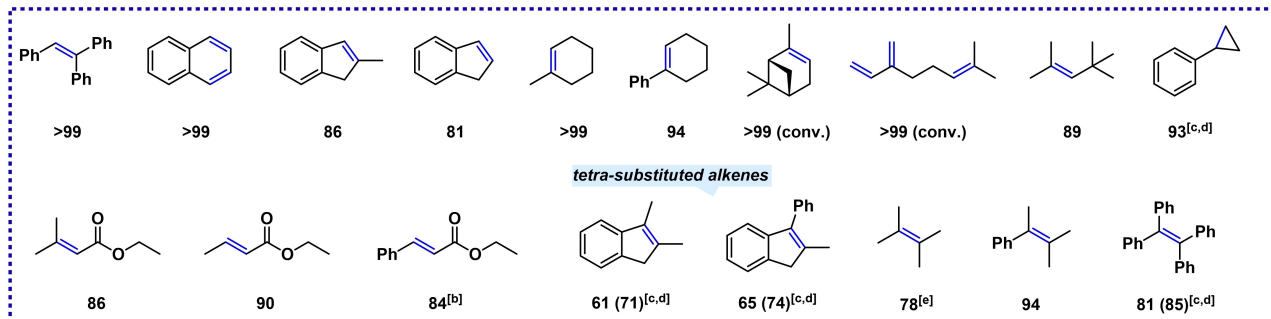


Figure 2. Hydrogenation of alkenes using **4**. Standard conditions: 0.2 mmol substrate (0.4 mol/L in THF). Protocol A: 3 mol% **4**, 2 bar H₂, 30 °C, 3 h. Protocol B: 5 mol% **4**, 12 bar H₂, 40 °C, 22 h. Yields and conversions were determined by quantitative GC-FID analysis vs. internal *n*-pentadecane. Conversions are given in parentheses if < 90%. [a] 8 bar H₂, 6 h. [b] solvent = PhMe. [c] V = 1.0 mL. [d] T = 60 °C. [e] only product calibrated due to solvent overlap of starting material in GC-FID.

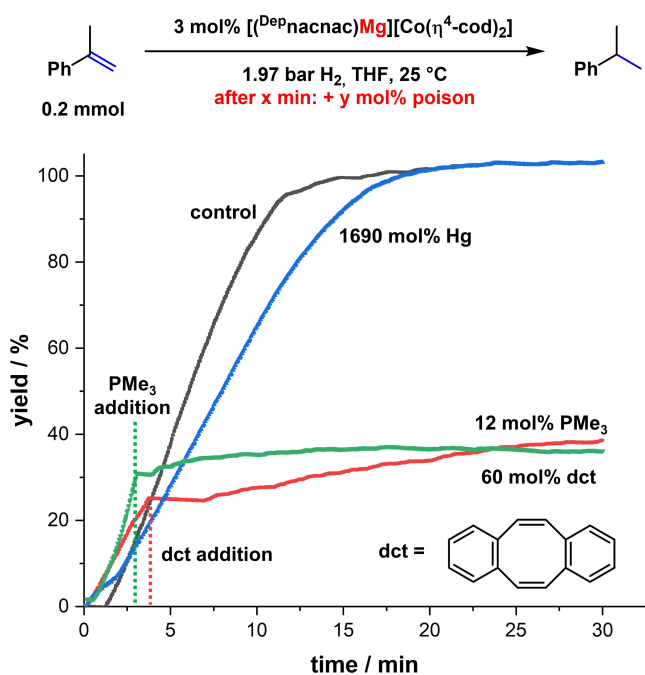


Figure 3. Kinetic poisoning studies with PMe₃, dct and Hg using pre-catalyst **4**.

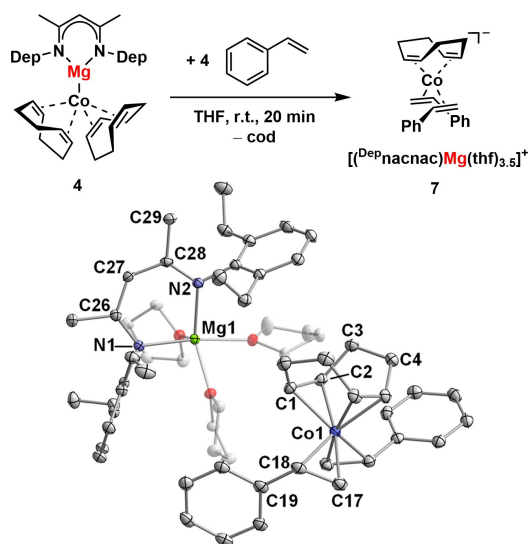
respect to **4**) resulted in catalyst inhibition (Figure 3, red curve). An excess of dct (10.0 equiv. per coordination site) is needed to suppress the hydrogenation of α -methylstyrene which can be attributed to the concomitant partial hydrogenation of dct.^[7] This is supported by the observation that the homoleptic dct complex [(^{Dep}nacnac)Mg][Co(η^4 -dct)₂](thf)_{1.7} (**6**) is also active in the hydrogenation of α -methylstyrene but with varying induction periods ranging from 0

to 10 min, while the addition of 60 mol % dct to **6** suppresses the hydrogenation activity (see the Supporting Information for details).^[24] Further investigation was conducted using protocol B (12 bar H₂ and 40 °C) to examine the potential formation of Co nanoparticles under these conditions. The presence of excess Hg had no impact on the hydrogenation of α , β -unsaturated esters, but varying outcomes were recorded for triphenylethylene (yielding 55–94 % of triphenylethane; see Table S4, SI). In this context, it is worth mentioning that an excess of Hg caused complete poisoning of an *in situ* generated Co nanoparticle catalyst under the same conditions (Table S4, SI).^[25]

In conclusion, a homotopic hydrogenation mechanism is consistent with these poisoning experiments for **4**. However, assessing catalyst topicity is intricate for anionic metalates, and the partial inhibition of the triphenylethylene hydrogenation using protocol B suggests that cobalt particles may contribute to some extent at elevated temperature and pressure.

Modelling Alkene Coordination

To model substrate coordination to the cobalt center, the bis(η^2 -styrene)cobaltate salt [(^{Dep}nacnac)Mg][Co(η^4 -cod)(η^2 -styrene)₂](thf)_{3.5} (**7**) was prepared in 43 % yield by reaction of **4** with 4.0 equiv. of styrene in THF (Scheme 2, top). SC-XRD analysis of crystals obtained from THF/*n*-hexane revealed a solvent-separated ion pair (Mg¹-Co1 7.509(2) Å), in which the (^{Dep}nacnac)Mg⁺ cation is coordinatively saturated with three THF molecules. The [(Co(η^4 -cod)(η^2 -styrene)₂)⁻ anion is bound in a distorted tetrahedral fashion to one η^4 -1,5-cyclooctadiene and two η^2 -styrene ligands (Scheme 2, bottom). Catalytic tests on the hydro-



Scheme 2. Top: Synthesis of $[(^{\text{Dep}}\text{nacnac})\text{Mg}][\text{Co}(\eta^4\text{-cod})(\eta^2\text{-styrene})_2]\cdot(\text{thf})_{3.5}$ (**7**). Bottom: Solid state molecular structure of **7**. Thermal ellipsoids are drawn at 40% probability level. H atoms and non-coordinated solvent molecules are omitted for clarity.

genation of selected alkenes using **7** (Table 2, toluene solvent) demonstrated comparable activity with respect to pre-catalyst **4** for α -methylstyrene (Table 2, Entry 1) and naphthalene (Table 2, Entry 4), while complex **7** was superior for 1,1,2,2-tetramethylethylene (Table 2, Entry 5; **4**: 78% vs. **6**: 98% yield). Thus, complex **7** presumably represents a substrate stabilized form of the active catalytic species.

Counterion Influence on Hydrogen Uptake

To gain further insight on the influence of the countercation on the reaction rate, we monitored the H_2 uptake for the α -methylstyrene hydrogenation reaction catalyzed by com-

plexes **1–4** (3 mol% pre-catalyst, 2 bar H_2 , 25 °C; Figure 4). The results show that the $(^{\text{Dep}}\text{nacnac})\text{Mg}^+$ salt **4** enabled the quantitative hydrogenation of the alkene substrate within 15 min (Figure 4a), while the Li^+ salt **3** gave $\approx 90\%$ yield after 30 min (Figure 4b). In contrast, the hydrogenation with K^+ salt **1** and Na^+ salt **2** gave only 16% and 32% yield, respectively, over a significantly longer time period (2 h) (Figure 4c, d). These observations are consistent with the reactivity trend observed for various other substrates (Table 1, see above). Furthermore, significant catalyst deactivation occurred for **1–3** between 10 and 20 min after the reaction onset, while the initial rate of hydrogenation also appeared to be lower with **1** and **2** than with **3** and **4**. These results illustrate the notable influence of the counter-cation on the catalytic activity. Since the hydrogenation of the cod ligand in the complexes might be a crucial factor contributing to their catalytic activity, the H_2 uptake of the complexes themselves was also monitored (2 bar H_2 , 25 °C, 1 h; Table 3 and the Supporting Information for further details) by quantifying the formation of cyclooctene and cyclooctane (which emerge from the uptake of one and two equiv. of H_2 , respectively) by GC-FID. The results show increasing H_2 incorporation by the cobaltate salts in the order $\mathbf{1} < \mathbf{2} < \mathbf{3} \approx \mathbf{4}$ (**1**: 12%, **2**: 24%, **3**: 45% **4**: 38%; Table 3, entries 1–4). In contrast, the hydrogenation of tetrabutylammonium cobaltate **5** gave only 1% H_2 incorporation (Table 3, entry 5), which indicates the need of an alkali metal or alkaline earth metal counterion for substantial hydrogenation activity. Remarkably, the heteroleptic complex **7** was fully hydrogenated when placed under an atmosphere of H_2 (Figure S4, SI), which is in line with its superior catalytic activity (see above) and suggests that the monodentate styrene ligand enables pre-catalyst hydrogenation under very mild conditions.

Table 2: Hydrogenation of alkenes with olefin cobaltates **4** and **7**.^[a]

Entry	Alkene	Conditions	Yield [%]	
			Cat. 4	Cat. 7
1		3 mol% cat., 2 bar H_2 , 30 °C, 3 h	> 99	> 99
2			> 99	> 99
3			90	93
4		5 mol% cat., 12 bar H_2 , 40 °C, 22 h	> 99	> 99
5			78	98

[a] Standard conditions: 0.2 mmol substrate (0.4 mol/L). Solvent = THF for pre-catalyst **4** and solvent = PhMe for pre-catalyst **7**. Yields were determined by quantitative GC-FID analysis vs. internal *n*-pentadecane.

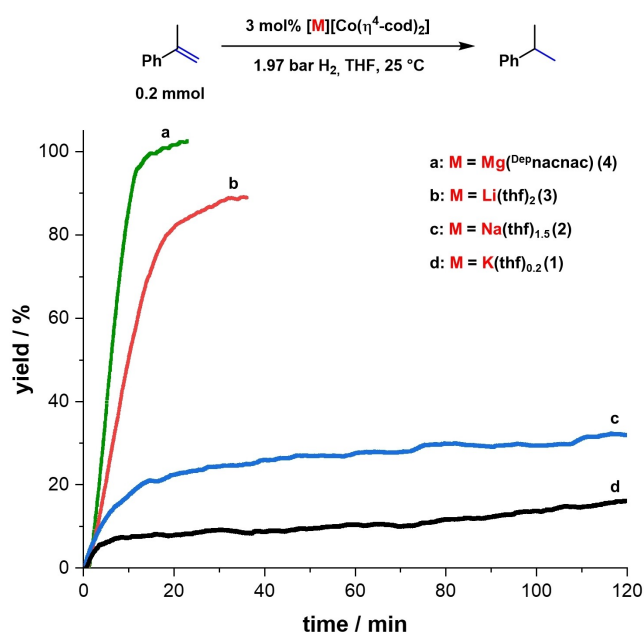


Figure 4. Reaction profile analysis of the hydrogenation of α -methylstyrene with pre-catalysts 1–4.

Computational Studies

To further understand the effect of the counterion, we performed a combined MM (molecular mechanics) MD simulation and DFT investigation to model the reaction mechanism and the interaction between the catalytically active anion and the cations. To begin, the whole reaction profile for the hydrogenation of styrene starting from anionic $[\text{Co}(\eta^4\text{-cod})(\eta^2\text{-styrene})_2]^-$ (7_A) was calculated at the DFT level ($r^2\text{SCAN-3c}$, $\text{CPCM}[\text{THF}]$) on the singlet surface and in the absence of any counterion (Scheme 3). Dissociation of one styrene molecule forms the 16 valence electron complex $[\text{Co}(\eta^4\text{-cod})(\eta^2\text{-styrene})]^-$ (8_A), which adds H_2 via oxidative addition ($9_A \rightarrow [10_A]^\ddagger \rightarrow 11_A$). Subsequent migratory

insertion of the styrene double bond into the Co-H bond of dihydride complex $[\text{Co}(\eta^4\text{-cod})(\eta^2\text{-styrene})\text{H}_2]^-$ ($11_A \rightarrow [12_A]^\ddagger \rightarrow 13_A$) is found to be the turnover-limiting step (TLS) with an activation barrier of 19.0 kcal/mol and a total energy barrier of 31.2 kcal/mol. The corresponding transition state structure is highly asynchronous with Pauling bond orders^[26] $\text{BO} = 0.95$ for the Co-C_2 bond and $\text{BO} = 0.54$ for the $\text{C}_1\text{-H}^a$ bond (see the structure of $[12_A]^\ddagger$ in Figure 5). Coordination of another styrene molecule precedes the reductive elimination of ethylbenzene from $[\text{Co}(\eta^4\text{-cod})(\eta^2\text{-styrene})(\text{H})(\text{CH}_2\text{CH}_2\text{Ph})]^-$ ($14_A \rightarrow [15_A]^\ddagger \rightarrow 8_A$), which drives the reaction downhill in energy ($\Delta G = -9.9$ kcal/mol).

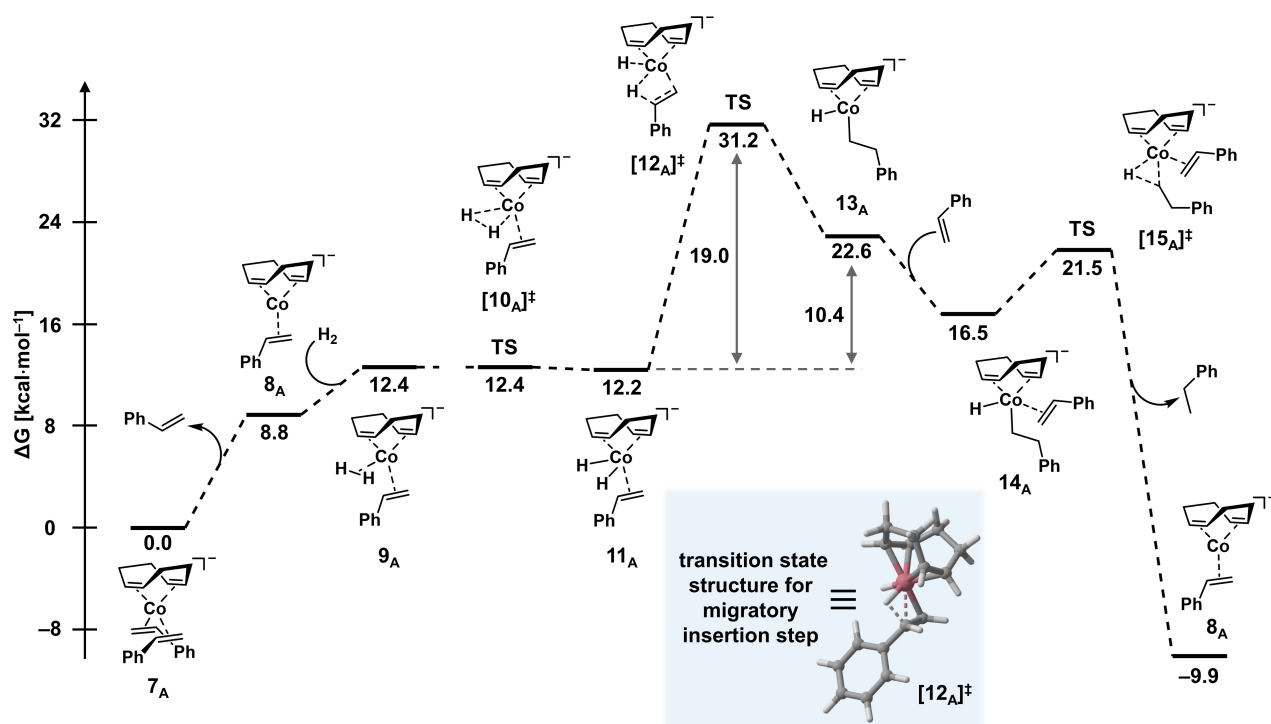
While this initial analysis established the elementary steps of the hydrogenation reaction, the anion-only model was not able to provide a reasonable total energy barrier (31.2 kcal/mol) for the hydrogenation of styrene at the experimental temperature of 298 K.^[27] Thus, we decided to investigate the influence of a metal-based counterion ($\text{M}^+ = \text{K}^+, \text{Na}^+, \text{Li}^+$ or $[\text{Depnacnac}]\text{Mg}^+$) on structures 11_A – 13_A in the turnover-limiting migratory insertion step. To adequately model the dynamic behavior of the solvated ion pairs $[\text{M}(\text{thf})_n][\text{Co}(\eta^4\text{-cod})(\eta^2\text{-styrene})\text{H}_2]^-$ (denoted as: 11_{K} , 11_{Na} , 11_{Li} and 11_{Mg}), force field based MD simulations were performed (see the SI). After initial force field parametrization, the time-dependent structural behavior of the system in a bulk of THF molecules ($n_{\text{THF}} \geq 500$) was studied and the most-populated ion pair structures were identified. According to the MD simulations, complexes 11_{K} to 11_{Mg} exhibit short distances between the metal cation and the cobalt anion indicating tight ion pairing.

To further characterize the counterion interactions within the migratory insertion step, the obtained geometries were then re-optimized at DFT level ($r^2\text{SCAN-3c}$) with explicit solvation in the first coordination sphere of the metal cation to capture solvent screening effects on the ion pair structures and energies. Intimate ion pairs were observed for complexes $11_{\text{K-Mg}}$; transition state structures $[12_{\text{K-Mg}}]^\ddagger$ and insertion products $13_{\text{K-Mg}}$. Figure 5 displays the transition state geometries for the migratory insertion step

Table 3: Hydrogenation of olefin cobaltates 1–5.^[a]

Pre-Catalyst ([Cation][Co(η^4 -cod) ₂])		cod	cod-H ₂	cod-H ₄	H ₂ Incorp.
$[\text{K}(\text{thf})_{0.2}]^+$	(1)	59	5	10	12
$[\text{Na}(\text{thf})_{1.5}]^+$	(2)	58	8	21	24
$[\text{Li}(\text{thf})_2]^+$	(3)	33	10	41	45
$[\text{Depnacnac}]\text{Mg}^+$	(4)	32	13	31	38
$[\text{N}(\text{t}^i\text{Bu})_4]^+$	(5)	88	1	0	1

[a] Standard conditions: 0.025 mmol pre-catalyst (0.05 mol/L THF). Substance ratios [%] and H₂ incorporation [%] were determined by quantitative GC-FID analysis vs. internal *n*-pentadecane as share of the overall hydrogenation mixture quantity. cod = 1,5-cyclooctadiene. cod-H₂ = cyclooctene. cod-H₄ = cyclooctane.



Scheme 3. Calculated reaction profile for the hydrogenation of styrene by anionic complex $[\text{Co}(\eta^4\text{-cod})(\eta^2\text{-styrene})_2]^-$ (**7_A**, level of theory: $r^2\text{SCAN-3c}$, CPCM[THF]).

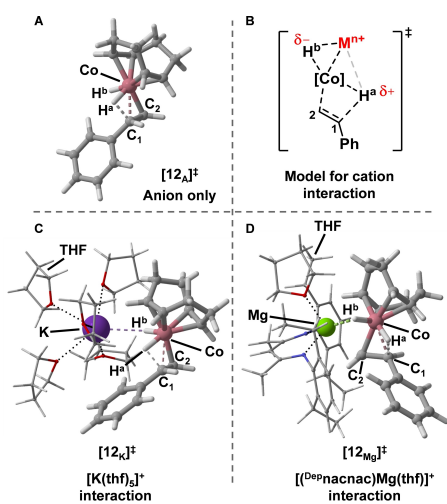


Figure 5. Transition state geometries of the turnover-limiting migratory insertion step. A: Anion only structure $[\mathbf{12}_A]^\ddagger$. B: Model for cation interaction. C: $[\text{K}(\text{thf})_5][\text{Co}(\eta^4\text{-cod})(\eta^2\text{-styrene})_2]$ structure ($[\mathbf{12}_K]^\ddagger$). D: $[(^{\text{Dep}})\text{nacnac}]\text{Mg}(\text{thf})[\text{Co}(\eta^4\text{-cod})(\eta^2\text{-styrene})_2]$ structure ($[\mathbf{12}_{\text{Mg}}]^\ddagger$).

for the pure anion $[\mathbf{12}_A]^\ddagger$ and the two potassium and magnesium cobaltate salts $[\text{K}(\text{thf})_5][\text{Co}(\eta^4\text{-cod})(\eta^2\text{-styrene})_2]$ ($[\mathbf{12}_K]^\ddagger$) and $[(^{\text{Dep}})\text{nacnac}]\text{Mg}(\text{thf})[\text{Co}(\eta^4\text{-cod})(\eta^2\text{-styrene})_2]$ ($[\mathbf{12}_{\text{Mg}}]^\ddagger$). The ion pairs $[\mathbf{12}_K]^\ddagger$ and $[\mathbf{12}_{\text{Mg}}]^\ddagger$ represent the two reactivity extremes for the alkali and alkaline earth metal cobaltate salts used in the hydrogenation reaction (see above). Direct cation hydride interactions are present in both transition states $[\mathbf{12}_K]^\ddagger$ and

$[\mathbf{12}_{\text{Mg}}]^\ddagger$ (and also in $[\mathbf{12}_{\text{Na/Li}}]^\ddagger$), while no cation styrene interaction can be observed (see the Supporting Information for the other ion pair structures). An analysis of the NPA charges for the pure anion $[\mathbf{12}_A]^\ddagger$ reveals a weak polarization of the two Co–H bonds with H^a exhibiting a slightly protic character whereas H^b is weakly hydridic (Figure 5, A and B; and Table 4, Entry A.5). This polarization difference of the Co– H^a /Co– H^b bond quantified by $\Delta\delta$ is already present in the intermediate structure **11_A** (Table 4, Entry A.4: 0.07) and is only slightly increased (to 0.14) in $[\mathbf{12}_A]^\ddagger$. In contrast, a stark increase $\Delta\delta$ is observed when a counterion is introduced in $[\mathbf{12}_{\text{K-Mg}}]^\ddagger$ (e.g. for Mg: Table 4, Entry E.4: 0.16 vs. E.5: 0.64). This can also be seen in the transition state geometries of $[\mathbf{12}_K]^\ddagger$ and $[\mathbf{12}_{\text{Mg}}]^\ddagger$, where H^b is directly oriented towards the metal cation thereby inducing a pronounced negative polarization in the Co– H^b bond (Figure 5, C and D).

The polarization difference $\Delta\delta$ in the transition state structures $[\mathbf{12}_{\text{K-Mg}}]^\ddagger$ was most pronounced for the magnesium salt $[\mathbf{12}_{\text{Mg}}]^\ddagger$ (Table 4, Entry A.5–E.5). This polarization may facilitate the migratory insertion of the alkene molecule. In addition, a distinct coordination geometry for $[\mathbf{12}_{\text{Mg}}]^\ddagger$ in comparison to $[\mathbf{12}_{\text{K-Li}}]^\ddagger$ was observed. While the alkali metal cobaltate salts exhibit a more central positioning of the cation between the two Co–H bonds (Figure 5C for $[\mathbf{12}_K]^\ddagger$), in $[\mathbf{12}_{\text{Mg}}]^\ddagger$ only the more hydridic H^b is in direct proximity to the magnesium cation (Figure 5D). Moreover, the benzyl unit of the styrene molecule is rotated outwards away from magnesium, while the benzyl group is oriented towards the alkali metal cation (Figure 5, C vs. D). Furthermore, a stepwise decrease in transition state energy (and thus total

Table 4: Key parameters for the reactivity differences for the migratory insertion step based on ground state structures $\mathbf{11}_A/\mathbf{11}_{K-Mg}$ and transition state structures $[\mathbf{12}_A]^\ddagger/[\mathbf{12}_{K-Mg}]^\ddagger$.

Entry	M^{n+}	A	B	C	D	E
		none	K^+	Na^+	Li^+	Mg^{2+}
1	ΔG^\ddagger ($[\mathbf{12}]^\ddagger$) [kcal/mol]	19.0 ^[a]	17.0	17.0	15.5	15.5
2	BO (Co–C ₂) ^[b]	0.95	0.95	0.95	0.97	0.90
3	BO (C ₁ –H ^a) ^[b]	0.54	0.60	0.61	0.61	0.55
4	$\Delta\delta$ ($\mathbf{11}$) ^[c]	0.07	0.14	0.13	0.16	0.16
5	$\Delta\delta$ ($[\mathbf{12}]^\ddagger$) ^[c]	0.14	0.58	0.55	0.55	0.64
6	r (M^{n+} –H ^b ; $[\mathbf{12}]^\ddagger$) [Å]	/	2.58	2.15	1.81	1.96

[a] Gibbs free energy derived from anion-only reaction profile calculation (Scheme 3). [b] Pauling bond orders using $c=0.6$ for TS structures.^[26] [c] Polarization difference of Co–H^a/Co–H^b bonds expressed by the differences of the natural population analysis (NPA) charges at H^a and H^b.

energy barrier) for the migratory insertion step corroborated the beneficial effect of the counterion (Table 4, A.1–E.1). A sequential decrease of the transition state energy in the order $[\mathbf{12}_A]^\ddagger > [\mathbf{12}_K]^\ddagger = [\mathbf{12}_{Na}]^\ddagger > [\mathbf{12}_{Li}]^\ddagger = [\mathbf{12}_{Mg}]^\ddagger$ is observed, which is in qualitative agreement with the observed reactivity trend of complexes **1–4**. In order to further examine the $[\text{Co–H}^b] \cdots M^+$ interaction, we conducted non-covalent interaction (NCI) analyses on the transition state structures $[\mathbf{12}_{K-Mg}]^\ddagger$ (Figure 6). The calculations were performed on the fully optimized geometries (r²SCAN-3c) and the electron densities calculated at ω B97M-V/def2-QZVP level of theory (see the Supporting Information for all NCI analyses). In all four transition state structures, an attractive

interaction between Co–H^b and the cation is observed. For $[\mathbf{12}_K]^\ddagger$, this interaction is indicated by the green isosurface between H^b and the potassium cation (Figure 6a) and by the green region in the two-dimensional NCI plot ($\text{sign}(\lambda_2)\rho < 0$; Figure 6b). Along the series of alkali metal cations, the attractive metal-hydride interaction becomes stronger following the trend: $K^+ < Na^+ < Li^+$ (Figure 6c for $[\mathbf{12}_{Na}]^\ddagger$, and Figure 6d for $[\mathbf{12}_{Li}]^\ddagger$). For lithium, a fairly strong interaction can be observed which is indicated by the additional blue color in the NCI isosurface and NCI plot cutout ($\text{sign}(\lambda_2)\rho \approx -0.3$; Figure 6d). The most pronounced attractive interaction was found between Co–H^b and the magnesium cation in $[\mathbf{12}_{Mg}]^\ddagger$ reaching into the range of strong non-covalent

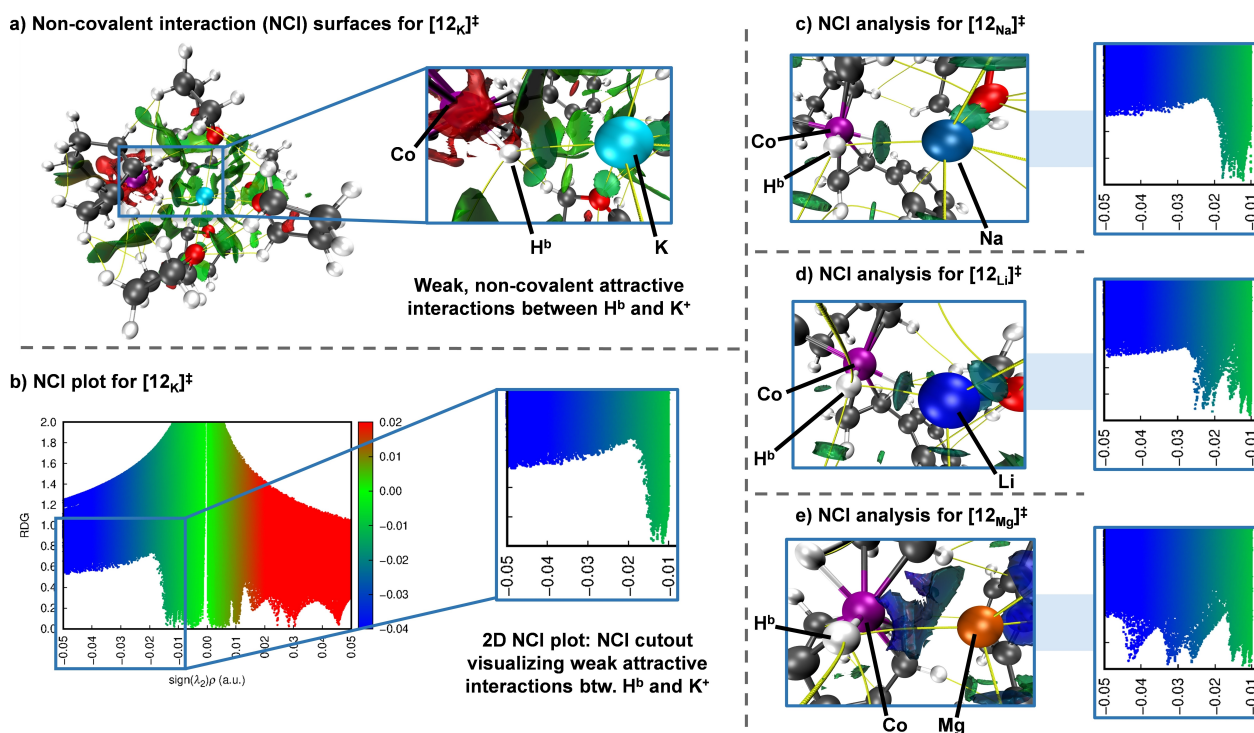


Figure 6. NCI-plots (2D) and surface visualization (3D) of $[\mathbf{12}_{K-Mg}]^\ddagger$. Diagrams show plots of RDG = reduced density gradient over $\text{sign}(\lambda_2)\rho$ = density with sign of the second derivative Hessian matrix. The $\text{sign}(\lambda_2)\rho > 0$ (red) are read as strong repulsive interactions, $\text{sign}(\lambda_2)\rho \approx 0$ (green) as weak interactions and $\text{sign}(\lambda_2)\rho < 0$ (blue) as strong attractive interactions.

interactions ($\text{sign}(\lambda_2)\rho \approx -0.5$; Figure 6e), thereby surpassing the hydride interaction with the alkali metal cations of $[\mathbf{12}_{\text{K-Li}}]^{\ddagger}$.

Overall, NCI analysis established an increasing attractive cation-hydride interaction following the trend: $\text{K}^+ < \text{Na}^+ < \text{Li}^+ < \text{Mg}^{2+}$. This trend is in agreement with the stronger bond polarization (Co-H^a vs. Co-H^b) found for the magnesium cobaltate salt, its reduced transition state energy for the turnover-limiting migratory insertion step and its distinct coordination geometry.

For completeness, the reductive elimination of styrene ($\mathbf{14} \rightarrow [\mathbf{15}]^{\ddagger}$) was analyzed in the same manner for the Na^+ and $(^{\text{Dep}}\text{nacnac})\text{Mg}^+$ salts (see the Supporting Information for details). This is the second elementary step to finalize the reduction of the styrene double bond. Even though this step is not turnover-limiting a distinct counterion effect on the transition state energy was observed for the more Lewis-acidic Mg^{2+} , while the sodium salt exhibited a near-identical reaction barrier ($[\mathbf{15}_{\text{Na}}]^{\ddagger}$) to the anion-only model. NCI analysis of $[\mathbf{15}_{\text{Mg}}]^{\ddagger}$ identified an interaction between the magnesium cation and the η^2 -bound styrene molecule, which likely accounts for the reduction in transition state energy. The accumulated computational data corroborates the heightened activity for magnesium cobaltate $\mathbf{4}$ (and $\mathbf{11}_{\text{Mg}}$) in the hydrogenation reactions which we observe experimentally.

Conclusion

This work shows that counterions have a remarkable effect on alkene hydrogenation reactions catalyzed by anionic cobalt complexes. The investigation of the series of $[\text{Cat}][\text{Co}(\eta^4\text{-cod})_2]$ complexes (Cat = K (**1**), Na (**2**), Li (**3**), $(^{\text{Dep}}\text{nacnac})\text{Mg}$ (**4**), $\text{N}(\text{tBu})_4$ (**5**)) revealed that the lithium and magnesium salts are much more powerful catalysts for the hydrogenation of challenging, highly substituted alkene substrates than the potassium and sodium salts. The presence of the non-coordinating tetrabutylammonium cation results in a sharp decrease in hydrogenation activity. $[(^{\text{Dep}}\text{nacnac})\text{Mg}][\text{Co}(\eta^4\text{-cod})_2]$ (**4**) showed the highest activity and to our knowledge is among the most active first-row transition metal catalysts for the hydrogenation of tri- and tetra-substituted alkenes.^[5b,f,h,i,7] In line with these catalytic investigations, reaction progress analyses and pre-catalyst hydrogenation experiments revealed differing reaction rates for the cobaltate salts **1** to **5**. The homotopic nature of the reaction mechanism was supported by poisoning studies. A combined MD and DFT study suggests the coordination of the counterion to the hydride in the turnover limiting migratory insertion step and demonstrates a beneficial, energy-lowering effect in comparison with the anion-only model system. The lowest energy barriers were calculated for $\text{M}=\text{Li}$ (**3**) and $\text{M}=(^{\text{Dep}}\text{nacnac})\text{Mg}$ (**4**). The NCI analyses of the migratory insertion transition state for complexes **1** to **4** illustrate the increasingly attractive interactions of the metal cations with one of the hydrido ligands following the trend: $\text{K}^+ (\mathbf{1}) < \text{Na}^+ (\mathbf{2}) < \text{Li}^+ (\mathbf{3}) < (^{\text{Dep}}\text{nacnac})\text{Mg}^+ (\mathbf{4})$, resulting in stronger Co–H bond polarization. The results of this

study show that counterion coordination can strongly modulate reactivity in hydrogenation reactions and possibly other catalytic reactions involving hydride intermediates. Furthermore, the nacnac ligand in **4** should enable the design of new structural motifs, such as asymmetric modifications. Investigations in these directions are ongoing.

Acknowledgements

We thank Dr. Gábor Balázs for valuable comments on the manuscript. The project received funding from the Deutsche Forschungsgemeinschaft (DFG, RTG 2620 IonPairs in Reaction Project 426795949). M.G. and F.G. thank the Fonds der Chemischen Industrie for a Kekulé Fellowship. Open Access funding enabled and organized by Projekt DEAL.

Conflict of Interest

The authors declare no conflict of interest.

Data Availability Statement

The data that support the findings of this study are available in the supplementary material of this article.

Keywords: Alkenes · Cobalt · Homogenous Catalysis · Hydrogenation · Ion Pairing

- [1] a) S. Nishimura, *Handbook of Heterogeneous Catalytic Hydrogenation for Organic Synthesis*, Wiley, New York **2001**; b) *The Handbook of Homogeneous Hydrogenation* (Eds.: J. G. de Vries, C. J. Elsevier), Wiley-VCH, Weinheim **2007**.
- [2] a) M. D. Garba, A. Galadima, *J. Phys. Sci.* **2018**, *29*, 153; b) T. Ohta, H. Takaya, M. Kitamura, K. Nagai, R. Noyori, *J. Org. Chem.* **1987**, *52*, 3174; c) M. K. Gupta, *Practical guide to vegetable oil processing*, Academic Press; AOCS Press, Amsterdam, Urbana, IL **2017**, p 171–215.
- [3] a) J. A. Osborn, F. H. Jardine, J. F. Young, G. Wilkinson, *J. Chem. Soc. A* **1966**, 1711; b) R. H. Crabtree, J. M. Mihelcic, J. M. Quirk, *J. Am. Chem. Soc.* **1979**, *101*, 7738; c) H. Doucet, T. Ohkuma, K. Murata, T. Yokozawa, M. Kozawa, E. Katayama, A. F. England, T. Ikariya, R. Noyori, *Angew. Chem. Int. Ed.* **1998**, *37*, 1703; d) T. Naota, H. Takaya, S.-I. Murahashi, *Chem. Rev.* **1998**, *98*, 2599.
- [4] a) P. J. Chirik, *Acc. Chem. Res.* **2015**, *48*, 1687; b) J. Loup, U. Dhawa, F. Pesciaoli, J. Wencel-Delord, L. Ackermann, *Angew. Chem. Int. Ed.* **2019**, *58*, 12803; c) L. Alig, M. Fritz, S. Schneider, *Chem. Rev.* **2019**, *119*, 2681; d) P. Gandeepan, T. Müller, D. Zell, G. Cera, S. Warratz, L. Ackermann, *Chem. Rev.* **2019**, *119*, 2192.
- [5] a) Q. Knijnenburg, A. D. Horton, H. van der Heijden, T. M. Kooistra, D. G. H. Hetterscheid, J. M. M. Smits, B. de Bruin, P. H. M. Budzelaar, A. W. Gal, *J. Mol. Catal. A* **2005**, *232*, 151; b) R. P. Yu, J. M. Darmon, J. M. Hoyt, G. W. Margulieux, Z. R. Turner, P. J. Chirik, *ACS Catal.* **2012**, *2*, 1760; c) S. Monfette, Z. R. Turner, S. P. Semproni, P. J. Chirik, *J. Am. Chem. Soc.* **2012**, *134*, 4561; d) M. R. Friedfeld, M. Shevlin,

- J. M. Hoyt, S. W. Krska, M. T. Tudge, P. J. Chirik, *Science* **2013**, *342*, 1076; e) T. N. Gieshoff, U. Chakraborty, M. Villa, A. Jacobi von Wangelin, *Angew. Chem. Int. Ed.* **2017**, *56*, 3585; f) N. G. Léonard, P. J. Chirik, *ACS Catal.* **2018**, *8*, 342; g) W. Ai, R. Zhong, X. Liu, Q. Liu, *Chem. Rev.* **2019**, *119*, 2876; h) Z. Wei, Y. Wang, Y. Li, R. Ferraccioli, Q. Liu, *Organometallics* **2020**, *39*, 3082; i) Y. Kobayashi, Y. Sunada, *ACS Sustainable Chem. Eng.* **2022**, *10*, 1078.
- [6] D. Gärtner, A. Welther, B. R. Rad, R. Wolf, A. Jacobi von Wangelin, *Angew. Chem. Int. Ed.* **2014**, *53*, 3722.
- [7] S. Sandl, T. M. Maier, N. P. van Leest, S. Kröncke, U. Chakraborty, S. Demeshko, K. Koszinowski, B. de Bruin, F. Meyer, M. Bodensteiner, C. Herrmann, R. Wolf, A. Jacobi von Wangelin, *ACS Catal.* **2019**, *9*, 7596.
- [8] T. M. Maier, S. Sandl, J. Melzl, J. Zweck, A. Jacobi von Wangelin, R. Wolf, *Chem. Eur. J.* **2020**, *26*, 6113.
- [9] P. Büschelberger, D. Gärtner, E. Reyes-Rodriguez, F. Kreyenschmidt, K. Koszinowski, A. Jacobi von Wangelin, R. Wolf, *Chem. Eur. J.* **2017**, *23*, 3139.
- [10] a) J. E. Ellis, *Inorg. Chem.* **2006**, *45*, 3167; b) W. W. Brennessel, J. E. Ellis, *Inorg. Chem.* **2012**, *51*, 9076; c) E. T. Ouellette, J. S. Magdalenksi, R. G. Bergman, J. Arnold, *Acc. Chem. Res.* **2022**, *55*, 783.
- [11] On cation effects in catalytic studies: a) C. R. Kennedy, S. Lin, E. N. Jacobsen, *Angew. Chem. Int. Ed.* **2016**, *55*, 12596; b) A. J. Neel, M. J. Hilton, M. S. Sigman, F. D. Toste, *Nature* **2017**, *543*, 637; c) A. Paparo, J. S. Silvia, T. P. Spaniol, J. Okuda, C. C. Cummins, *Chem. Eur. J.* **2018**, *24*, 17072; d) T. V. Tran, L. J. Karas, J. I. Wu, L. H. Do, *ACS Catal.* **2020**, *10*, 10760; e) T. X. Gentner, A. R. Kennedy, E. Hevia, R. E. Mulvey, *ChemCatChem* **2021**, *13*, 2371; f) A. H. Farquhar, K. E. Gardner, S. Acosta-Calle, A. M. Camp, C.-H. Chen, A. J. M. Miller, *Organometallics* **2022**, *41*, 3366; g) A. M. Borys, E. Hevia, *Dalton Trans.* **2023**, *52*, 2098; h) S. Acosta-Calle, A. J. M. Miller, *Acc. Chem. Res.* **2023**, *56*, 971; i) P. A. Macdonald, S. Banerjee, A. R. Kennedy, A. van Teijlingen, S. D. Robertson, T. Tuttle, R. E. Mulvey, *Angew. Chem. Int. Ed.* **2023**, *62*, e202304966.
- [12] On cation effects in synthetic studies: a) J. Andrez, V. Guidal, R. Scopelliti, J. Pécaut, S. Gambarelli, M. Mazzanti, *J. Am. Chem. Soc.* **2017**, *139*, 8628; b) D. L. J. Broere, B. O. Mercado, E. Bill, K. M. Lancaster, S. Sproules, P. L. Holland, *Inorg. Chem.* **2018**, *57*, 9580; c) S. M. Bhutto, P. L. Holland, *Eur. J. Inorg. Chem.* **2019**, 1861; d) A. Najafian, T. R. Cundari, *Inorg. Chem.* **2019**, *58*, 12254; e) G. M. Ballmann, M. J. Evans, T. X. Gentner, A. R. Kennedy, J. R. Fulton, M. P. Coles, R. E. Mulvey, *Inorg. Chem.* **2022**, *61*, 19838; f) A. Rae, K. M. Byrne, S. A. Brown, A. R. Kennedy, T. Krämer, R. E. Mulvey, S. D. Robertson, *Chem. Eur. J.* **2022**, *28*, e202104260; g) S. Banerjee, P. A. Macdonald, S. A. Orr, A. R. Kennedy, A. van Teijlingen, S. D. Robertson, T. Tuttle, R. E. Mulvey, *Chem. Eur. J.* **2022**, *28*, e202201085; h) A. Logallo, E. Hevia, *Chem. Commun.* **2023**, *59*, 5383; i) M. J. Evans, C. Jones, *Inorg. Chem.* **2023**, *62*, 14393–14401; j) H.-Y. Liu, M. S. Hill, M. F. Mahon, C. L. McMullin, R. J. Schwamm, *Organometallics* **2023**, *42*, 2881.
- [13] M. R. Kita, A. J. M. Miller, *Angew. Chem. Int. Ed.* **2017**, *56*, 5498.
- [14] a) F. Freitag, T. Irrgang, R. Kempe, *J. Am. Chem. Soc.* **2019**, *141*, 11677; b) G. Zhang, T. Irrgang, M. Schlagbauer, R. Kempe, *Chem Catal.* **2021**, *1*, 681.
- [15] P. A. Dub, J. C. Gordon, *Nat. Chem. Rev.* **2018**, *2*, 396.
- [16] a) K. Jonas (Studiengesellschaft Kohle mbH), US4169845 A, **1977**; b) K. Jonas, R. Mynott, C. Krüger, J. C. Sekutowski, Y.-H. Tsay, *Angew. Chem.* **1976**, *88*, 808.
- [17] J. A. Kelly, J. Gramüller, R. M. Gschwind, R. Wolf, *Dalton Trans.* **2021**, *50*, 13985.
- [18] a) J. A. Widegren, R. G. Finke, *J. Mol. Catal. A* **2003**, *198*, 317; b) C. A. Jaska, I. Manners, *J. Am. Chem. Soc.* **2004**, *126*, 9776; c) R. H. Crabtree, *Chem. Rev.* **2012**, *112*, 1536; d) D. Gärtner, S. Sandl, A. Jacobi von Wangelin, *Catal. Sci. Technol.* **2020**, *10*, 3502.
- [19] An almost immediate reaction onset was observed for the hydrogenation of α -methylstyrene with **7** (Figure S4, SI). Here, the cobaltate motif is coordinated by one η^5 -1,5-cyclooctadiene and two η^2 -styrene ligands. Ligand exchange and pre-catalyst hydrogenation is significantly facilitated due to the (monodentate) styrene ligands which reduces the induction period to a minimum.
- [20] Note that an initial induction period can be in part due to the experimental set up (pressure increase when the last solution is added to the reaction vessel and thus initial consumption of this over-pressure at the start of the measurement).
- [21] a) P. J. Dyson, *Dalton Trans.* **2003**, 2964; b) V. Artero, M. Fontecave, *Chem. Soc. Rev.* **2013**, *42*, 2338; On amalgamation with metals: c) C. Gumiński, *J. Mater. Sci.* **1989**, *24*, 3285; d) H. R. Kirchmayr, *Monatsh. Chem.* **1964**, *95*, 1479.
- [22] On quantitative phosphine and phosphite poisoning of iron group metals: a) K.-N. T. Tseng, J. W. Kampf, N. K. Szymczak, *ACS Catal.* **2015**, *5*, 411; b) S. Sandl, F. Schwarzhuber, S. Pöllath, J. Zweck, A. Jacobi von Wangelin, *Chem. Eur. J.* **2018**, *24*, 3403.
- [23] Note that the hydrogenation of α -methylstyrene with 3 mol % **4** and 3 mol % PMe_3 led to additional hydrogenation of the phenyl moiety, giving fully reduced isopropylcyclohexane in 42 % yield (see the Supporting Information for further details). This is in accordance with previous reports on arene hydrogenation by transition metal phosphine and phosphite complexes: a) E. L. Muetterties, F. J. Hirsekorn, *J. Am. Chem. Soc.* **1974**, *96*, 4063; b) M. C. Rakowski, F. J. Hirsekorn, L. S. Stuhl, E. L. Muetterties, *Inorg. Chem.* **1976**, *15*, 2379; c) L. S. Stuhl, M. Rakowski DuBois, F. J. Hirsekorn, J. R. Blecke, A. E. Stevens, E. L. Muetterties, *J. Am. Chem. Soc.* **1978**, *100*, 2405; d) E. L. Muetterties, J. R. Blecke, *Acc. Chem. Res.* **1979**, *12*, 324; e) K. Jonas, *Angew. Chem. Int. Ed.* **1985**, *24*, 295; f) M. D. Fryzuk, J. B. Ng, S. J. Rettig, J. C. Huffman, K. Jonas, *Inorg. Chem.* **1991**, *30*, 2437.
- [24] Contrasting the reactivity of **6**, the known potassium salt $[\text{K}(\text{thf})_2][\text{Co}(\eta^4\text{-dct})_2]$ was not able to hydrogenate related alkenes (e.g. styrene) under 2 bar H_2 at ambient temperature overnight.^[9] This observation once more underscores the substantial impact of the $(^{\text{Dep}}\text{nacnac})\text{Mg}^+$ cation on the hydrogenation activity. Furthermore, it seems noteworthy that both **6** and $[\text{K}(\text{thf})_2][\text{Co}(\eta^4\text{-dct})_2]$ do not undergo ligand exchange with styrene in the absence of H_2 (see the Supporting Information for details). These observations suggest that ligand hydrogenation in the pre-catalysts initiates the formation of the catalytically active species.
- [25] P. Büschelberger, E. Reyes-Rodriguez, C. Schöttle, J. Treptow, C. Feldmann, A. Jacobi von Wangelin, R. Wolf, *Catal. Sci. Technol.* **2018**, *8*, 2648.
- [26] a) L. Pauling, *J. Am. Chem. Soc.* **1947**, *69*, 542.
- [27] a) H. Ryu, J. Park, H. K. Kim, J. Y. Park, S.-T. Kim, M.-H. Baik, *Organometallics* **2018**, *37*, 3228; b) L. N. Mendelsohn, L. Pavlovic, H. Zhong, M. R. Friedfeld, M. Shevlin, K. H. Hopmann, P. J. Chirik, *J. Am. Chem. Soc.* **2022**, *144*, 15764.
- [28] Deposition numbers 2294851 (for **2**), 2294850 (for **5**), 2294808 (for **6**), 2294852 (for **7**), and 2294852 (for $[(^{\text{Dep}}\text{nacnac})\text{Mg}(\text{OMe})_2]$) contain the supplementary crystallographic data for this paper. These data are provided free of charge by the joint Cambridge Crystallographic Data Centre and Fachinformationszentrum Karlsruhe Access Structures service.

Manuscript received: October 12, 2023

Accepted manuscript online: December 7, 2023

Version of record online: January 4, 2024